Epigenetic regulation of *EIF4A1* through DNA methylation and an oncogenic role of eIF4A1 through BRD2 signaling in prostate cancer

Chao Wang[1],

Jonathan Leavenworth[1],

Chao Zhang[1],

Zhichao Liu[1],

Katherine Y. Yuan[1],

Yichun Wang[1],

Guangxin Zhang[1],

Shuaibin Wang[1],

Xuelian Cui[1],

Yue Zhang[1],

Sejong Bae[2,3],

Jiangbing Zhou[4,5],

Lizhong Wang[1,2],

Runhua Liu[1,2]

[1]Department of Genetics, University of Alabama at Birmingham, Birmingham, AL

[2]Department of O'Neal Comprehensive Cancer Center, University of Alabama at Birmingham, Birmingham, AL

[3]Department of Medicine, University of Alabama at Birmingham, Birmingham, AL

[4]Department of Neurosurgery, Yale University, New Haven, CT.

[5]Department of Biomedical Engineering, Yale University, New Haven, CT.

Abstract

In prostate cancers, elongation initiation factor 4A1 (eIF4A1) supports an oncogenic translation program and is highly expressed, but its role remains elusive. By use of human specimens and

Corresponding Authors: Runhua Liu, the University of Alabama at Birmingham, 720 20th Street South, Birmingham, AL 35294, runhua@uab.edu; Lizhong Wang, lwang12@uab.edu.

Conflict of interest statement: There are no potential conflicts of interest for disclosure.

cell models, we addressed the role of eIF4A1 in prostate cancer *in vitro* and *in vivo*. *EIF4A1* expression, as determined by mRNA and protein levels, was higher in primary prostate cancers relative to normal prostate tissue. Also, for primary prostate cancers, elevated mRNA levels of *EIF4A1* correlated with DNA hypomethylation levels in the CpG-rich island of *EIF4A1*. Using a DNMT3a CRISPR-Cas9-based tool for specific targeting of DNA methylation, we characterized, in human prostate cancer cells, the epigenetic regulation of *EIF4A1* transcripts through DNA methylation in the CpG-rich island of *EIF4A1*. Next, we investigated the oncogenic effect of *EIF4A1* on cancer cell proliferation *in vitro* and tumor growth *in vivo*. For prostate cancer cells, *EIF4A1* heterozygous knockout or knockdown inhibited protein translation and tumor growth. In addition, using RNA immunoprecipitation with RNA sequencing, we discovered the eIF4A1-mediated translational regulation of the oncogene *BRD2*, which contains the most enriched eIF4A1-binding motifs in its 5' untranslated region, establishing an eIF4A1-BRD2 axis for oncogenic translation. Finally, we found a positive correlation between expression levels of eIF4A1 and BRD2 in primary prostate cancers. Our results demonstrate, for prostate cancer cells, epigenetic regulation of *EIF4A1* transcripts through DNA methylation and an oncogenic roles of eIF4A1 through BRD2 signaling.

Keywords

EIF4A1; prostate cancer; tumor progression; oncogene

Introduction

A defining characteristic of many types of cancer is the dysregulation of mRNA translation [1], which may drive the oncogenic phenotype to promote tumor progression. mRNA translation can be separated into three distinct stages: initiation, elongation, and termination. Initiation factors have recently been targeted in anti-oncogenic therapeutic strategies, including those for prostate cancer [2]. The initiation step of translation is regulated by the mRNA-bearing elongation initiation factor 4F (eIF4F) complex, including eIF4A, 4B, 4G, and 4E. eIF4A is the ATP-dependent helicase that unwinds secondary structures in the 5' untranslated region (5' UTR) of mRNA before translation occurs [3]. The eIF4A family consists of 3 closely related proteins, eIF4A1, A2, and A3. eIF4A1 unwinds secondary and tertiary structures of G-quadruplexes in the 5' UTR to facilitate translation of coded proteins [4]. Of note, in cancers, RNA G-quadruplexes promote eIF4A-dependent oncogene translation [5]. However, it remains to be determined whether eIF4A1 contributes to the progression of prostate cancers.

In transformed, prostate-derived epithelial cell lines, most oncogenes are translationally upregulated relative to normal prostate epithelial cells [6]. Additionally, for efficient translation, many of these genes require helicases to unwind secondary and tertiary structures in the 5' UTR [5]. eIF4A1 supports an oncogenic translation program and may alter the translation of prostate cancer-associated oncogenes that contain G-quadruplexes or other consensus sequences within their mRNAs [5, 7, 8]. In the present study, we characterized the expression profile and epigenetic regulation of *EIF4A1* in human prostate cancer specimens and cell lines. Also, we addressed its functional role on cell growth and

progression of prostate cancers. Finally, we identified potential regulatory targets of eIF4A1 and relevant mechanisms in the regulation of translation.

Results and Discussion

EIF4A1 expression is increased in human prostate cancers through epigenetic regulation by DNA hypomethylation in the promoter region of *EIF4A1*

As determined with The Cancer Genome Atlas (TCGA) dataset, expression of *EIF4A1* was upregulated in most human cancers (15/24), including prostate cancer (Fig. S1A). As shown in mass-spectrometry-based proteomic data from the Clinical Proteomic Tumor Analysis Consortium (CPTAC) dataset, expression of the eIF4A1 protein was higher in most human cancers as compared to normal controls (Fig. S1B). In TCGA prostate adenocarcinomas, there was elevated expression of *EIF4A1* in prostate cancer tissues relative to normal prostate tissue (Fig. 1A). Of note, high expression of *EIF4A1* was associated with poor survival of patients with prostate cancer (Fig. 1B). In our sample cohort, we evaluated, by immunohistochemistry (IHC), expression of the eIF4A1 protein and assessed its relationship with tumor progression in 85 prostate cancer tissues with 13 high-grade prostatic intraepithelial neoplasia (PIN) tissues and 85 tumor-adjacent normal prostate tissues (Table S1). All positive samples expressed cytoplasmic eIF4A1, but a few samples showed both cytoplasmic and nuclear staining. Approximately 85% (72/85) of the tumor-adjacent normal prostate tissues had no or low eIF4A1 expression, and only 15% (13/85) had high levels of eIF4A1 expression (H-score > 50) (Fig. 1C and 1D). However, 40% (34/85) of the prostate cancer samples had high levels of eIF4A1 expression (H-score > 50) (Figs. 1C and 1D). Although, in localized tumors, the expression of eIF4A1 increased with tumor stage (T1 to T3), it was lower in metastatic tumors (T4 or N+ or M+) (Fig. 1E), suggesting an upregulation of eIF4A1 in early-stage prostate cancers. Also, we characterized the effect of eIF4A1 on tumor aggressiveness. Expression of eIF4A1 was not associated with Gleason scores (Fig. 1F). Likewise, in the Human Protein Atlas dataset (www.proteinatlas.org), eIF4A1 was expressed in 60% (6/10) of prostate cancers but not in normal prostates (0/3); the difference, however, was not statistically significant (Figs. S1C and S1D).

Next, we used the cBioPortal dataset (www.cbioportal.org) to perform a genetic analysis of *EIF4A1* in 7677 prostate adenocarcinoma samples from 13 studies. Only a few genetic alterations (average < 4%) of *EIF4A1*, including amplification, deletion, and mutation, were found in human prostate adenocarcinomas (Fig. S2). However, DNA methylation levels in the promoter region of *EIF4A1* were lower in prostate adenocarcinomas relative to normal prostate controls (Fig. 1G). Of note, for prostate adenocarcinomas, expression levels of *EIF4A1* negatively correlated with DNA methylation levels ($r = -0.534$, $p < 0.001$, Fig. 1H), suggesting epigenetic regulation of *EIF4A1* transcripts by DNA methylation in these cancers. Then, we identified a prominent 5'CpG island (1414-bp, 136 CpG sites) of *EIF4A1* using the UCSC Genome Browser (genome.ucsc.edu) (Fig. 1I). Bisulfite sequencing was used to identify, in DU145 cells, DNA hypomethylation at the CpG island of *EIF4A1* and high expression of eIF4A1 (Figs. 1N and 2A). To test whether promoter DNA methylation regulates *EIF4A1* transcription, we utilized a CRISPR-dCas9 (a catalytically dead Cas9)-

DNMT3a construct, which provides a simple way to acquire gene-specific modifications of DNA methylation, to establish dCas9-DNMT3a stably expressing DU145 cells (Fig. 1K). Three single guide RNAs (sgRNAs) targeting the *EIF4A1* promoter were designed to guide the dCas9-DNMT3a for the *EIF4A1*-specific DNA methylation (Fig. 1J). The DU145 cells stably expressing dCas9-DNMT3a were transiently transduced by sgRNAs, and the sgRNA-transfected cells were sorted by flow cytometry for transcription and DNA methylation analyses (Figs. 1K and 1L). As shown in Fig. 1M, sgRNA transduction reduced transcription of *EIF4A1* in the DU145 cells stably expressing dCas9-DNMT3a. Bisulfite sequencing confirmed induced DNA methylation in the CpG sites of *EIF4A1* at day 6 after sgRNA transduction (Figs. 1N and S3). These data suggest that, in prostate cancer cells, induction of DNA methylation of the *EIF4A1* promoter inhibits transcription of *EIF4A1*.

EIF4A1 heterozygous knockout (KO) inhibits protein translation and tumor growth in an androgen-independent manner

eIF4A1 was highly expressed in two castration-resistant prostate cancer (CRPC) cell lines, DU145 and PC3, and one androgen-dependent cell line, LNCaP (Figs. 2A, 2G and 2O). In DU145 and PC3 cells, eIF4A1 was expressed in the cytoplasm (Figs. S4A and S4B). To determine its functional role in prostate cancer cells, we knocked out *EIF4A1* in DU145 and PC3 cells using CRISPR/Cas9 genome editing, and then the KO clones were selected by Western blots, Sanger sequencing, and polysomal profiling. Although a few selected clones showed homozygous KO of *EIF4A1*, all KO clones died after 2 or 3 generations in cell culture, indicating that *EIF4A1* homozygous KO is lethal in prostate cancer cells. To address this issue, we selected clones with CRISPR heterozygous KO of *EIF4A1* (*EIF4A1*$^{+/-}$) by Sanger sequencing (Fig. S4C). In these *EIF4A1*$^{+/-}$ cells, expression of eIF4A1 protein was low (Figs. 2A and 2G). Cell proliferation and colony numbers were also low compared to scramble-treated DU145 cells, but these effects were reversed by exogenous transfection with *EIF4A1* (Figs. 2B–F). This phenotype was also validated in *EIF4A1*$^{+/-}$ PC3 cells (Figs. 2H–J). To establish the effect of *EIF4A1* on tumor growth *in vivo*, *EIF4A1* scramble-treated and *EIF4A1*$^{+/-}$ DU145 cells were subcutaneously injected into male immunodeficient NSG mice. At day 27 after inoculation, xenograft tumor growth was slower in mice injected with *EIF4A1*$^{+/-}$ DU145 cells than in mice injected with scramble-treated cells (Fig. 2K). At day 27, tumor weights were also low in mice injected with *EIF4A1*$^{+/-}$ DU145 cells compared to those injected with scramble-treated cells (Figs. 2L and 2M). In addition, in *EIF4A1*$^{+/-}$ DU145 cells relative to scramble-treated cells, there were, in polysome graphs, 3 peaks for the 40S and 60S ribosomal subunits and 80S monosomes with a chain of actively translating mature ribosomal complexes. Polysomal profiling showed a lower abundance of polysomes, indicating inhibition of translating activity (Fig. 2N). Likewise, there was inhibition of growth of LNCaP cells after knockdown of *EIF4A1* by small interfering RNAs (siRNAs) (Figs. 2O and 2P). However, *EIF4A1*-mediated growth of LNCaP cells was not blocked by androgen depletion (Fig. 2Q). Thus, their growth was androgen-independent.

Identification of translational targets and relevant signaling of eIF4A1 in human prostate cancer cells

In cancers, RNA G-quadruplexes cause eIF4A-dependent oncogene translation [5], but whether key oncogenes and their translation are regulated by eIF4A1 in prostate cancer

remains elusive. Thus, we screened the translational targets of eIF4A1 in DU145 cells using Native RNA Immunoprecipitation (RIP) assays with RNA-seq (RIP-seq). As shown in Fig. 3A, RIP-seq was performed in paired sets with eIF4A1- and IgG-derived IPs. The eIF4A1-binding peaks and RNA fractions were normally distributed around the ATG translation start site (Figs. 3B and 3C). In the eIF4A1-RIP sample, 197 coding genes with eFI4A1-binding peaks in mRNAs, including the 5' UTR, exon, and 3' UTR regions, were identified (Fig. 3B). The top 3 most enriched eFI4A1-binding motifs (MAGGTA, CCASCYC, and GARGA) were identified by aligning the sequences of all eFI4A1-binding RNA fractions to a reference genome (Fig. 3D). Next, we identified 14 coding genes with long and complicated 5' UTRs, which contained the top enriched eIF4A1-binding motifs in their 5' UTRs (Fig. 3E). Of 14 coding genes, 6 genes, including *BRD2, HIF1A, PPP1R2, TRIP12, TSC22D4,* and *ZER1,* were confirmed with RIP-quantitative PCR (qPCR) for more mRNA transcripts in the eIF4A1-RIP sample compared to the IgG-RIP sample (Fig. 3E). Of note, in DU145 cells, eIF4A1-binding peaks with increased mRNA transcripts were found in mRNAs of three bromodomain and extraterminal (BET) family genes, *BRD2, BRD3,* and *BRD4* (Figs. 3F, 3G and S5A–C). However, eIF4A1-binding peaks in the 5' UTR with top enriched motifs were identified only in *BRD2* (Figs. S5B and S5D). Furthermore, in the prostate cancer cell lines, DU145, PC3, and LNCaP, eIF4A1-binding RNA fractions and top enriched motifs in their 5' UTRs with increased mRNA transcripts were validated for three genes, *BRD2, HIF1A,* and *TSC22D4*, by use of RIP-qPCR with specific primers within the 5' UTR (Figs. 3G–I).

The BET family is essential for epigenetic regulation of target genes and cancer cell growth, and BET inhibitors are promising therapeutic agents for patients with metastatic CRPC [9, 10]. In various cancers, c-MYC (also referred to as MYC) is a transcriptional target of the BET family [11], and targeting the BET-MYC axis overcomes androgen resistance in metastatic CRPC [12]. In TCGA dataset, increased expression of *MYC*, *BRD2*, and *BRD3*, but not *BRD4*, was evident in prostate cancer tissues relative to normal prostate tissues (Fig. S6A). Furthermore, among prostate cancers, we identified a positive correlation of expression of *EIF4A1* with expression of *MYC*, *BRD2*, and *BRD4*, but not *BRD3* (Fig. S6B). In the PCTA dataset, however, this correlation was validated for *EIF4A1* only with *MYC* and *BRD2* (Fig. S6C). As determined by Western blots, protein expression levels of BRD2, BRD3, BRD4, and MYC in DU145 and PC3 cells were lower after *EIF4A1* heterozygous KO (Figs. 4A–C). Thus, we identified, for prostate cancer cells, eIF4A1-mediated translation initiation of the oncogene *BRD2* (Fig. S5D). To further validate the eIF4A1-BRD2 axis, we transfected EIF4A1 into DU145 and PC3 *EIF4A1*$^{+/-}$ cells. As shown in Figs. S7A and S7B, expression levels of BRD2 protein in these cells were rescued after *EIF4A1* transfection.

The MYC protein, an oncogenic transcription factor, targets a large gene network, leading to changes in expression of many genes that regulate the cell cycle, survival, protein synthesis, cell adhesion, and metabolism [13–15]. To determine if the expression of *EIF4A1* correlates with MYC signaling in prostate cancer tissues, we analyzed TCGA and PCTA datasets for an expression correlation of *EIF4A1* with MYC target genes identified in previous studies [16, 17]. As shown in Fig. S8, there were significant correlations between the expression levels of *EIF4A1* and MYC target genes, including *TMPRSS2, CDKN2B, MCL1, RIOX2,*

PTMA, LDHA, ODC1, APEX1, FASN, FKBP4, HSPD1, NCL, NPM1, ODC1, PTMA, RPL23, RPL6, and *TPM1.* In prostate cancers, these genes are essential for cell growth, apoptosis, and metabolism [15–17]. Although, in our RIP assays, eIF4A1 did not interact with MYC directly (Fig. 3), eIF4A1 may regulate the MYC signaling through BRD2 in human prostate cancer.

We further evaluated other potential eIF4A1-regulated translational targets and relevant signaling using public datasets and protein expression analyses. In prostate cancers, there was a positive correlation between expression levels of *EIF4A1* and *HIF1A* in the PCTA dataset but not in TCGA dataset (Figs. S6D and S6E). Also, in normoxia, there was no change of HIF1α expression in the DU145 and PC3 EIF4A1+/− cells compared to scrambled control cells (Figs. S9A and S9B). Since HIF1α is more stabilized in low oxygen concentrations or hypoxia [18], we performed this experiment in hypoxia condition. Although protein expression of HIF1α was lower after *EIF4A1* heterozygous KO in DU145 cells under hypoxia, this reduction was not evident in *EIF4A1*$^{+/-}$ PC3 cells (Figs. 4A–C). Also, in prostate cancers, there was no correlation between the mRNA expression levels of *EIF4A1* and *TSC22D4* (Figs. S6D and S6E). Likewise, in DU145 and PC3 cells, protein expression of TSC22D4 was not appreciably changed after *EIF4A1* heterozygous KO (Figs. 4A–C). The eIF4F complex and its inhibitors regulate translation initiation for oncogenes, such as those encoding cyclins (e.g., cyclin D1) and anti-apoptotic proteins (e.g., BCL2 and BCLXL) [5, 19]. In our analysis, lower protein expression of cyclin D1, BCL2, and BCLXL was evident in *EIF4A1*$^{+/-}$ DU145 and PC3 cells (Figs. 4A–C). However, as shown by RIP-seq and RIP-qPCR analyses of DU145 cells, eIF4A1 did not bind directly to the 5′ UTRs in mRNAs of these genes (Fig. S5C).

Co-expression of eIF4A1 and BRD2 in prostate cancer samples

Since our data showed eIF4A1-mediated translational regulation of BRD2 in prostate cancer cells, we assessed the expression of eIF4A1 and BRD2 and their association in prostate cancer xenografts and primary cancers. In DU145 mouse xenografts, protein expression of eIF4A1 and BRD2 was less in *EIF4A1*$^{+/-}$ tumors than in scramble-transfected tumors (Fig. 4D). In primary prostate cancers, H-score analysis showed a positive correlation between expression levels of eIF4A1 and BRD2 ($r = 0.529$, $p < 0.0001$) (Figs. 4E and 4F), suggesting co-expression of these factors in human prostate cancers.

eIF4A1, a DEAD-box RNA helicase, accelerates the translation of certain transcripts that contain consensus structural sequences within their 5' UTRs; these structures are more common among oncogenes [5, 20]. In breast cancers, eIF4A is involved in the malignant phenotype, including cell proliferation, survival, stemness, cell cycle progression, angiogenesis, and chemoresistance [21–23]. In gastric cancers, high intratumoral expression of eIF4A1 promotes the epithelial-to-mesenchymal transition and is positively associated with poor tumor differentiation, advanced tumor stage, and poor prognosis [24]. Likewise, in TCGA dataset, there is overexpression of *EIF4A1* in most human cancers, and this is associated with poor survival for patients with various cancers (Figs. 1B, S1A and S10). As seen in the present study, *EIF4A1* heterozygous KO inhibits protein translation and growth of prostate cancer cells in an androgen-independent manner, supporting an oncogenic role

for *EIF4A1* in prostate cancer. In our IHC analysis, expression of eIF4A1 was high for tumor stages T1 to T3 but not in metastatic tumors. Thus, eIF4A1 is most likely an initiator of oncogenic transformation for tumor progression but not a necessary regulator for metastasis of prostate cancer.

The mechanism of transcription regulation of *EIF4A1* and its overexpression in prostate cancer remains unknown. An early study found a CpG-rich, methylation-free island in the first intron of *EIF4A1* [25]. In the UCSC Genome Browser, we identified a CpG-rich island between the proximal promoter and the first intron of *EIF4A1.* In TCGA dataset, hypomethylation levels in this CpG-rich island correlated with high expression levels of *EIF4A1* mRNA in human prostate cancers. In the present study, our functional analysis by DNMT3a CRISPR-targeted DNA methylation revealed that DNA methylation in this CpG-rich island is responsible for expressing the *EIF4A1* transcripts, supporting an epigenetic regulation of *EIF4A1* transcripts by DNA methylation in human prostate cancer cells.

eIF4A recognizes specific motifs of mRNAs that contain G-quadruplex sequences with secondary structure in their 5' UTRs [5, 20]. eIF4A1 also targets regions other than G-quadruplexes of mRNAs and promotes mRNA translation through classical secondary structures [7, 26]. In the present study, using native RIP-seq with the DREME algorithm, we identified the top 3 enriched 7-, 6-, and 5-nucleotide motifs among the eFI4A1-binding peaks. Only our identified 7-nucleotide motif CCASCYC was relatively more GC-rich, which is similar to the previously reported (CGG)4 or G(CGG)3CR motifs [5, 20] (Fig. S11). Furthermore, eFI4A1-binding peaks were enriched in the mRNAs of the BET gene family, including *BRD2*, *BRD3*, and *BRD4*. However, only the long 5' UTR of *BRD2,* which contains multiple top nucleotide motifs, interacted with eIF4A1, and eIF4A1-mediated expression of BRD2 was validated in prostate cancer cells. For *BRD3* and *BRD4*, eFI4A1-binding peaks were found only in exons of these genes. In addition, we identified two other eFI4A1 target genes, *HIF1A* and *TSC22D4.* eFI4A1 binds to their long 5' UTRs, which contain eFI4A1-binding motifs. However, eIF4A1-mediated expression of HIF1α and TSC22D4 was not validated in DU145 or PC3 cells.

eIF4A facilitates translation of oncogenic mRNAs, leading to the synthesis of oncoproteins, such as cyclin D1, Bcl2, MCL1, MUC1, ROCK1, ARF6, HDM2, BIRC5, and survivin, which are essential for tumor cell survival, proliferation, migration, invasion, metastasis, and chemoresistance [27–30]. However, in the present study with DU145 cells, no eFI4A1-binding peaks were identified in the 5' UTRs of these genes. Our native RIP assay has an advantage and a disadvantage. Its advantage is identifying the targets as they interact with eIF4A1 in the cytosol during their native state. The disadvantage is that the eIF4A1 is associated with the cytoplasmic lysates freely and may bind to multiple targets, or even to different places on the same target. Our data demonstrate that eIF4A1 not only interacts with the 5' UTR but may bind to other sites on the transcript. Also, mRNA may recruit the eIF4A1 protein at the time a ribosome decodes mRNA to produce a protein. *In vitro,* the protein configuration can be altered, potentially creating eIF4A1-recognizable structures that would not exist *in vivo*. Thus, our data need to be validated by various technologies *in vitro* and *in vivo*. Also, further investigation of prostate cancers is required to identify additional eIF4A1-mediated oncogenic drivers.

BRD2, as a target of AR signaling, is induced by androgen stimulation in prostate cancer cells, and expression of BRD2 is positively associated with mortality for patients with prostate cancer [31]. In the present study, we discovered that *BRD2* contains multiple eIF4A1-binding consensus sequences in its long 5' UTR, directly associated with the eIF4A1 RIP. Also, in TCGA dataset, expression of *BRD2* positively correlated with those of *EIF4A1*. In the present study, there was co-expression of eIF4A1 and BRD2 proteins in prostate cancers, supporting existence of an eIF4A1-BRD2 axis for oncogenic translation in human prostate cancers. BRD2 is a transcriptional activator of MYC [11]. However, our data showed that, in prostate cancer cells, eIF4A1 was unlikely to interact with MYC directly. Thus, in these cells, eIF4A1 may drive androgen-independent cell growth through BRD2-MYC signaling.

In summary, eIF4A1, an androgen-independent initiator of oncogenic transformation, is highly expressed in human prostate cancers through an epigenetic regulation involving DNA hypomethylation. During translation initiation in prostate cancer cells, eIF4A1 interacts with a transcript in the 5' UTR of *BRD2* mRNA to facilitate protein translation, which may drive the oncogenic phenotype of prostate cancer.

Materials and Methods

Generation of CRISPR-dCas9 (a catalytically dead Cas9)-DNMT3a cell line

The Fuw-dCas9-Dnmt3a construct (Addgene, Plasmid #84476), in which dCas9 is fused with DNA methylase DNMT3a, was used to generate CRISPR-dCas9-DNMT3a stably expressing DU145 cell line for CRISPR-dCas9-targeted DNA methylation of the *EIF4A1* promoter as described previously [32]. sgRNAs were cloned into the pLenti U6- pgRNA (mCherry)-modified (Addgene, Plasmid #84477), as described previously [32], to generate sgRNA lentiviral expression constructs. sgRNA target sequences are listed in Table S2. Next, the CRISPR/dCas9 stably expressing cell lines were transduced with sgRNA lentiviruses. After transduction, cells were sorted by fluorescence-activated cell sorting using a BD FACS Aria2 with mCherry (sgRNA) for CRISPR-dCas9-targeted DNA methylation analysis.

RNA immunoprecipitation (RIP)

Cells (10^6) were cultured on 2×100 mm^2 plates to reach 70% confluency. After washing in ice-cold PBS, cells were collected by scraping into cytoplasmic extract buffer, protease inhibitor cocktail, and RNAseOut then collected, lysed, and pelleted. The supernatant was transferred to fresh tubes and snap-frozen to −80°C. When prepared, lysates were incubated with pre-swollen beads to clear non-specific interactions and pelleted. Ten percent of the supernatant was collected for "input", the remainder was split into two paired tubes for rabbit anti-eIF4A1 or control rabbit IgG IP. Antibody and beads were allowed to conjugate at 2 hours on ice, and then mixed with lysate. The paired mixtures were incubated for 6 hours to overnight at 4°C with gentle rotation (antibody - bead with lysate). The lysate was pelleted and washed x 6 times and then total RNA was isolated using the TRIzol RNA isolation protocol.

RNA library preparation and sequencing

RNA libraries were prepared using TruSeq Stranded mRNA Library Prep Kits (Illumina, San Diego, CA) according to the manufacturer`s protocol. Integrity was assessed using an Agilent 2200 Tapestation instrument (Agilent Technologies, Santa Clara, CA). First-strand cDNA syntheses were performed using random hexamers and ProtoScript II Reverse Transcriptase (New England Biolabs, Ipswich, MA). The libraries were normalized, pooled, and subjected to cluster and pair-read sequencing performed for 150 cycles on a HiSeqX10 instrument (Illumina), according to the manufacturer's instructions. The RNA-seq data were submitted to NCBI GEO (accession No. GSE161709).

Identification of eFI4A1-binding peaks and motifs

There were pairwise sequence data from two RNA-seq samples (eIF4A1 and IgG). The quality check was performed on each sample. The samples were aligned against GRch38Decoy reference genome using BWA (http://bio-bwa.sourceforge.net). The peaks were identified in the alignment using MACS2 [33, 34]. The peaks were called on RIP-eIF4A1 using RIP-IgG as a control. The peaks were annotated using R package ChIPseeker [35]. The bed files were produced by the MACS2 and expanded the region to 50 bp using bed tools to create expanded bed files. These files were then used to extract the corresponding sequences from the genomes using bed tools. Finally, the motifs were found using DREME (http://meme-suite.org/doc/dreme.html).

Other materials and methods is referred to the supplemental data.

Supplementary Material

Refer to Web version on PubMed Central for supplementary material.

Acknowledgements

References

1. Malina A, Mills JR, Pelletier J. Emerging therapeutics targeting mRNA translation. Cold Spring Harb Perspect Biol 2012; 4: a012377.

2. Ramamurthy VP, Ramalingam S, Kwegyir-Afful AK, Hussain A, Njar VC. Targeting of protein translation as a new treatment paradigm for prostate cancer. Curr Opin Oncol 2017: 210–220. [PubMed: 28282343]

3. Jackson RJ, Hellen CU, Pestova TV. The mechanism of eukaryotic translation initiation and principles of its regulation. Nat Rev Mol Cell Biol 2010; 11: 113–127. [PubMed: 20094052]

4. Sonenberg N, Hinnebusch AG. Regulation of translation initiation in eukaryotes: mechanisms and biological targets. Cell 2009; 136: 731–745. [PubMed: 19239892]

5. Wolfe AL, Singh K, Zhong Y, Drewe P, Rajasekhar VK, Sanghvi VR et al. RNA G-quadruplexes cause eIF4A-dependent oncogene translation in cancer. Nature 2014; 513: 65–70. [PubMed: 25079319]

6. Schrecengost R, Knudsen KE. Molecular pathogenesis and progression of prostate cancer. Semin Oncol 2013; 40: 244–258. [PubMed: 23806491]

7. Waldron JA, Tack DC, Ritchey LE, Gillen SL, Wilczynska A, Turro E et al. mRNA structural elements immediately upstream of the start codon dictate dependence upon eIF4A helicase activity. Genome Biol 2019; 20: 300. [PubMed: 31888698]

8. Chan K, Robert F, Oertlin C, Kapeller-Libermann D, Avizonis D, Gutierrez J et al. eIF4A supports an oncogenic translation program in pancreatic ductal adenocarcinoma. Nat Commun 2019; 10: 5151. [PubMed: 31723131]

9. Asangani IA, Dommeti VL, Wang X, Malik R, Cieslik M, Yang R et al. Therapeutic targeting of BET bromodomain proteins in castration-resistant prostate cancer. Nature 2014; 510: 278–282. [PubMed: 24759320]

10. Faivre EJ, McDaniel KF, Albert DH, Mantena SR, Plotnik JP, Wilcox D et al. Selective inhibition of the BD2 bromodomain of BET proteins in prostate cancer. Nature 2020; 578: 306–310. [PubMed: 31969702]

11. Muhar M, Ebert A, Neumann T, Umkehrer C, Jude J, Wieshofer C et al. SLAM-seq defines direct gene-regulatory functions of the BRD4-MYC axis. Science 2018; 360: 800–805. [PubMed: 29622725]

12. Kregel S, Malik R, Asangani IA, Wilder-Romans K, Rajendiran T, Xiao L et al. Functional and Mechanistic Interrogation of BET Bromodomain Degraders for the Treatment of Metastatic Castration-resistant Prostate Cancer. Clin Cancer Res 2019; 25: 4038–4048. [PubMed: 30918020]

13. Dang CV. c-Myc target genes involved in cell growth, apoptosis, and metabolism. Mol Cell Biol 1999; 19: 1–11. [PubMed: 9858526]

14. Dang CV, O'Donnell KA, Zeller KI, Nguyen T, Osthus RC, Li F. The c-Myc target gene network. Semin Cancer Biol 2006; 16: 253–264. [PubMed: 16904903]

15. Remondini D, O'Connell B, Intrator N, Sedivy JM, Neretti N, Castellani GC et al. Targeting c-Myc-activated genes with a correlation method: detection of global changes in large gene expression network dynamics. Proc Natl Acad Sci U S A 2005; 102: 6902–6906. [PubMed: 15867157]

16. Ellwood-Yen K, Graeber TG, Wongvipat J, Iruela-Arispe ML, Zhang J, Matusik R et al. Myc-driven murine prostate cancer shares molecular features with human prostate tumors. Cancer Cell 2003; 4: 223–238. [PubMed: 14522256]

17. Zeller KI, Jegga AG, Aronow BJ, O'Donnell KA, Dang CV. An integrated database of genes responsive to the Myc oncogenic transcription factor: identification of direct genomic targets. Genome Biol 2003; 4: R69. [PubMed: 14519204]

18. Kumar A, Vaish M, Karuppagounder SS, Gazaryan I, Cave JW, Starkov AA et al. HIF1alpha stabilization in hypoxia is not oxidant-initiated. Elife 2021; 10: e72873.

19. De Benedetti A, Graff JR. eIF-4E expression and its role in malignancies and metastases. Oncogene 2004; 23: 3189–3199. [PubMed: 15094768]

20. Modelska A, Turro E, Russell R, Beaton J, Sbarrato T, Spriggs K et al. The malignant phenotype in breast cancer is driven by eIF4A1-mediated changes in the translational landscape. Cell Death Dis 2015; 6: e1603. [PubMed: 25611378]

21. de la Parra C, Walters BA, Geter P, Schneider RJ. Translation initiation factors and their relevance in cancer. Curr Opin Genet Dev 2018; 48: 82–88. [PubMed: 29153484]

22. Raman D, Tiwari AK. Role of eIF4A1 in triple-negative breast cancer stem-like cell-mediated drug resistance. Cancer Rep (Hoboken) 2020: e1299.

23. Sridharan S, Robeson M, Bastihalli-Tukaramrao D, Howard CM, Subramaniyan B, Tilley AMC et al. Targeting of the Eukaryotic Translation Initiation Factor 4A Against Breast Cancer Stemness. Front Oncol 2019; 9: 1311. [PubMed: 31867270]

24. Gao C, Guo X, Xue A, Ruan Y, Wang H, Gao X. High intratumoral expression of eIF4A1 promotes epithelial-to-mesenchymal transition and predicts unfavorable prognosis in gastric cancer. Acta Biochim Biophys Sin (Shanghai) 2020; 52: 310–319. [PubMed: 32147684]

25. Quinn CM, Wiles AP, El-Shanawany T, Catchpole I, Alnadaf T, Ford MJ et al. The human eukaryotic initiation factor 4AI gene (EIF4A1) contains multiple regulatory elements that direct

high-level reporter gene expression in mammalian cell lines. Genomics 1999; 62: 468–476. [PubMed: 10644445]

26. Waldron JA, Raza F, Le Quesne J. eIF4A alleviates the translational repression mediated by classical secondary structures more than by G-quadruplexes. Nucleic Acids Res 2018; 46: 3075–3087. [PubMed: 29471358]

27. Malka-Mahieu H, Newman M, Desaubry L, Robert C, Vagner S. Molecular Pathways: The eIF4F Translation Initiation Complex-New Opportunities for Cancer Treatment. Clin Cancer Res 2017; 23: 21–25. [PubMed: 27789529]

28. Leppek K, Das R, Barna M. Functional 5' UTR mRNA structures in eukaryotic translation regulation and how to find them. Nat Rev Mol Cell Biol 2018; 19: 158–174. [PubMed: 29165424]

29. Rubio CA, Weisburd B, Holderfield M, Arias C, Fang E, DeRisi JL et al. Transcriptome-wide characterization of the eIF4A signature highlights plasticity in translation regulation. Genome Biol 2014; 15: 476. [PubMed: 25273840]

30. Jin C, Rajabi H, Rodrigo CM, Porco JA, Jr., Kufe D. Targeting the eIF4A RNA helicase blocks translation of the MUC1-C oncoprotein. Oncogene 2013; 32: 2179–2188. [PubMed: 22689062]

31. Urbanucci A, Barfeld SJ, Kytola V, Itkonen HM, Coleman IM, Vodak D et al. Androgen Receptor Deregulation Drives Bromodomain-Mediated Chromatin Alterations in Prostate Cancer. Cell Rep 2017; 19: 2045–2059. [PubMed: 28591577]

32. Liu XS, Wu H, Ji X, Stelzer Y, Wu X, Czauderna S et al. Editing DNA Methylation in the Mammalian Genome. Cell 2016; 167: 233–247 e217. [PubMed: 27662091]

33. Zhang Y, Liu T, Meyer CA, Eeckhoute J, Johnson DS, Bernstein BE et al. Model-based analysis of ChIP-Seq (MACS). Genome Biol 2008; 9: R137. [PubMed: 18798982]

34. Feng J, Liu T, Qin B, Zhang Y, Liu XS. Identifying ChIP-seq enrichment using MACS. Nat Protoc 2012; 7: 1728–1740. [PubMed: 22936215]

35. Yu G, Wang LG, He QY. ChIPseeker: an R/Bioconductor package for ChIP peak annotation, comparison and visualization. Bioinformatics 2015; 31: 2382–2383. [PubMed: 25765347]
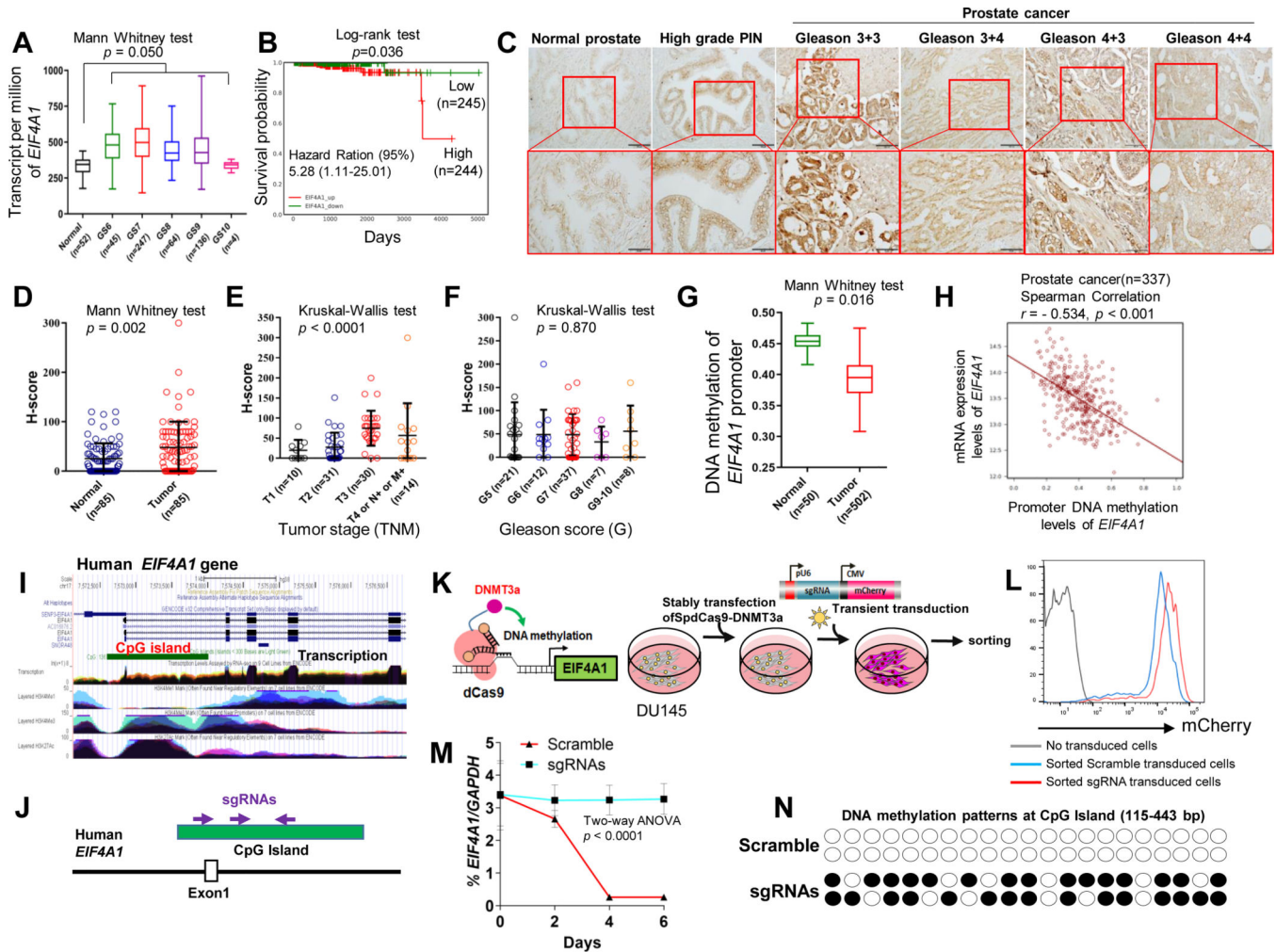
Figure 1. Expression and promoter DNA methylation of *EIF4A1* and its epigenetic regulation in human prostate cancer.

(**A**) Differential expression levels of *EIF4A1* between normal prostate tissues with Gleason grades and prostate cancer tissues from TCGA dataset. Data are presented as the medians and interquartile ranges. (**B**) Kaplan-Meier curves, log-rank test, and Cox proportional hazards regression for *EIF4A1* expression at low and high levels in prostate cancers from TCGA dataset through the Prostate Cancer Transcriptome Atlas (PCTA) database. (**C**) Representative immunohistochemical (IHC) staining in normal prostate, high-grade prostatic intraepithelial neoplasia (PIN), and prostate cancer tissues with anti-human EIF4A1 mAb (Abcam, ab31217). The percentage of positive tumor cells per slide (0% to 100%) was multiplied by the dominant intensity pattern of staining (1, weak; 2, moderate; 3, intense); therefore, the overall H-score ranged from 0 to 300. (**D-F**) Quantitative H-scores for tumor-adjacent normal prostate samples and prostate cancer samples with tumor stages and Gleason scores. (**G**) DNA methylation levels in the CpG island of the *EIF4A1* promoter between normal prostate and prostate cancer tissues from TCGA dataset. Data are presented as the medians and interquartile ranges. (**H**) Correlation of mRNA expression levels of *EIF4A1* with DNA methylation levels in the CpG island of the *EIF4A1* promoter in prostate cancer samples from TCGA dataset. (**I**) Screenshot from the UCSC genome browser

showing location of the *EIF4A1* promoter, CpG island, exons, intron1, and transcription and histone marks. (**J**) Single guide RNAs (sgRNAs) for guiding CRISPR/dCas9-DNMT3a to target the CpG island of the *EIF4A1* promoter. (**K** and **L**) Experimental procedure for the stable transduction of CRISPR/dCas9-DNMT3a, transient transduction of scramble empty vector or sgRNA vectors, and cell sorting of mCherry expressing DU145 cells. (**M**) Quantitative expression analysis of *EIF4A1* before and after sgRNA transduction of CRISPR/dCas9-DNMT3a cells at days 0, 2, 4, and 6 as determined by qPCR. The fold change in expression was calculated using the $2^{-\Delta\Delta Ct}$ method with *GAPDH* mRNA as an internal control. (**N**) DNA methylation status at the CpG island before and after sgRNA transduction of CRISPR/dCas9-DNMT3a into DU145 cells at day 6 as determined by bisulfite sequencing. Open and full black circles show unmethylated and methylated CpG sites, respectively. This experiment was repeated three times.
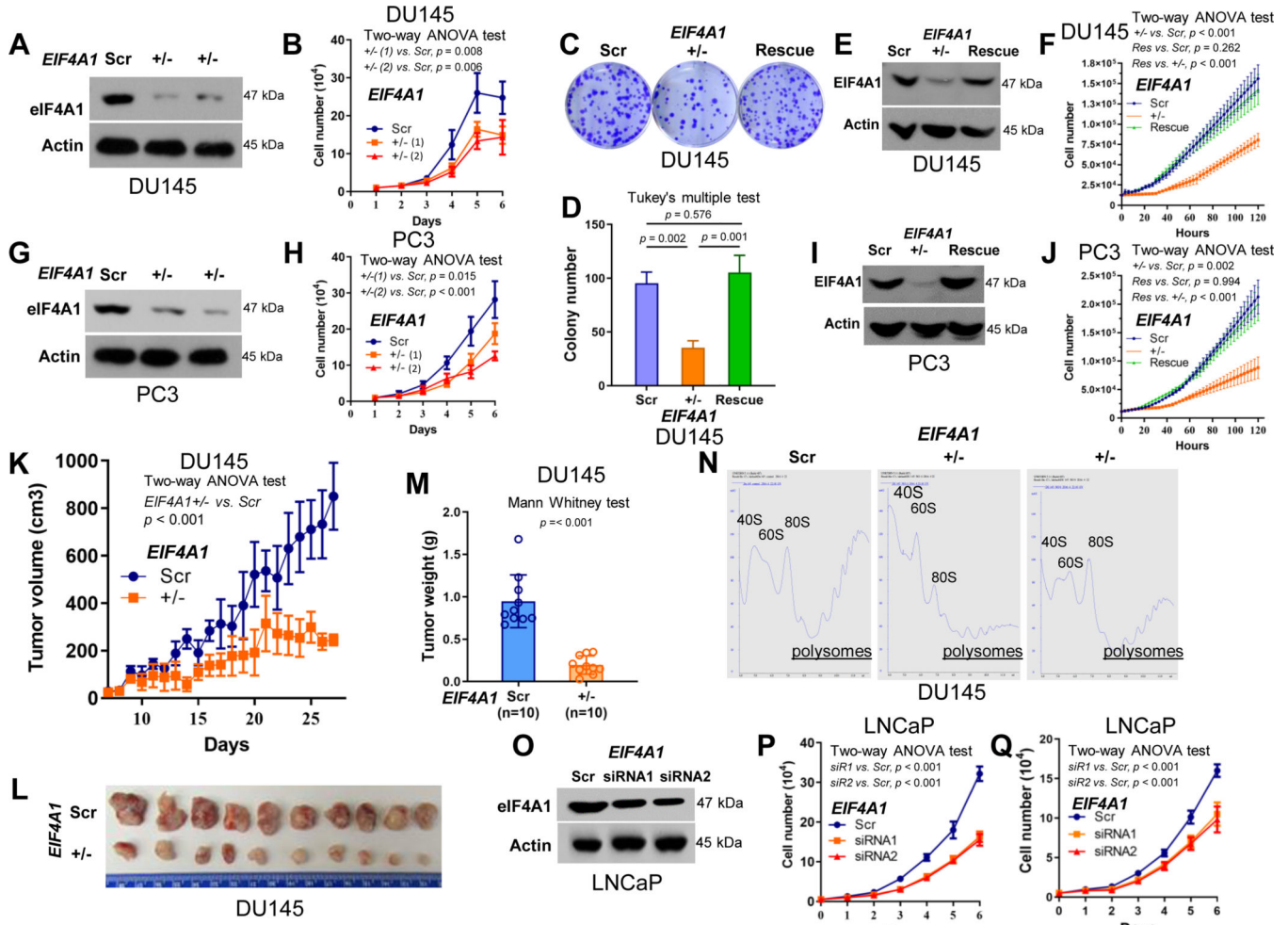
Figure 2. Effect of *EIF4A1* heterozygous knockout or knockdown on cell proliferation, tumor growth, and translating activity in human prostate cancer cells.
(**A, E, G, I**) Downregulation and rescue of eIF4A1 expression in *EIF4A1* heterozygous knockout (*EIF4A1*$^{+/-}$) DU145 and PC3 cells, verified by Western blots. (**B-D, F**) Cell proliferation assay and colony formation assay for DU145 cells. (**F, J**) Cell proliferation assay for PC3 cells. (**K**) Tumor volumes in NSG mice after injection (n=10/group). (**M, L**) Representative tumor masses and mean tumor weights on day 27 after injection. (**N**) Polysome profiles of *EIF4A1*$^{+/-}$ clones against a scramble-treated control in DU145 cells. Free ribosomal subunits (40S and 60S), monosomes (80S), and polysomes in the polysome fractions are indicated. (**O**) Knockdown of eIF4A1 in LNCaP cells by *EIF4A1* small interfering RNAs (siRNAs) verified by Western blots. Growth of LNCaP cells transfected with *EIF4A1* siRNAs in androgen-included (**P**) or androgen-depleted (**Q**) culture medium. Data are presented as the means and standard deviation (SD). Scr, scramble. All experiments were repeated three times.
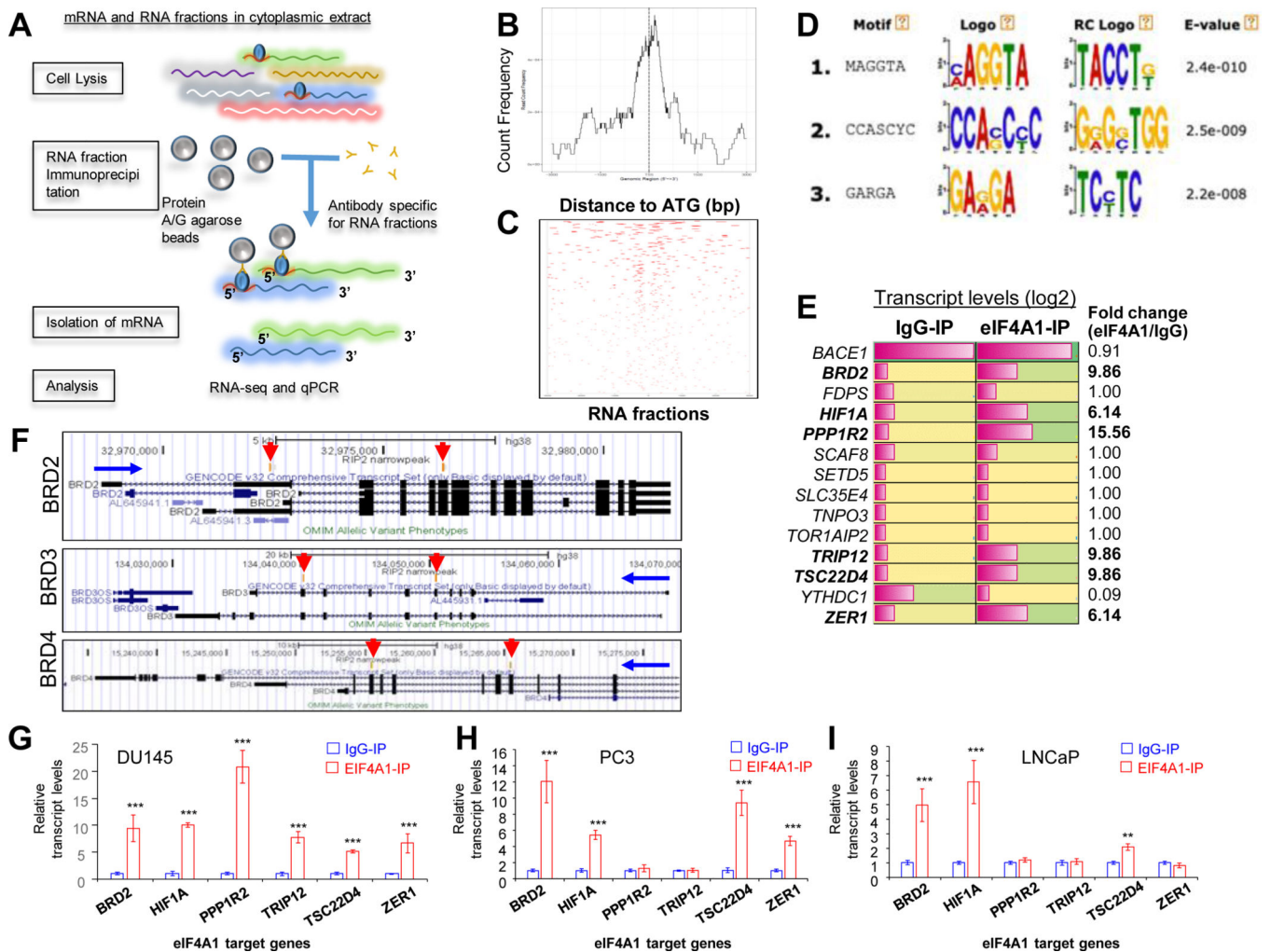
Figure 3. Identification of eIF4A1 target mRNAs in the 5' UTR of genes and their binding motifs in human prostate cancer cells.

(**A**) The workflow of the RIP assay. (**B, C**) Heat-map and distribution of eIF4A1-RIP-seq peaks and RNA fractions in the ATG translation start site of target genes. Peaks are in the top plot and RNA fractions in the bottom plot. (**D**) Top 3 enriched eIF4A1-binding motifs from sequences in eIF4A1-binding sites. (**E**) Expression levels of IgG- or eIF4A1-RIP transcripts in the 5' UTRs of candidate genes. (**F**) eIF4A1-binding sites (red arrows) in the transcription regions of *BRD2*, *BRD3*, and *BRD4*. Screenshot from the UCSC genome browser showing locations of the promoter, exons (including 5' UTR and 3' URT), introns, and transcription direction (blue arrows). (**G-I**) IRP-qPCR validation of eIF4A1-binding peaks in the 5' UTRs of candidate genes in DU145, PC3, and LNCaP cells, as determined by qPCR. Data are presented as the means and SD. **p<0.01, ***p<0.001 by a two-tailed *t*-test. All experiments were repeated three times.
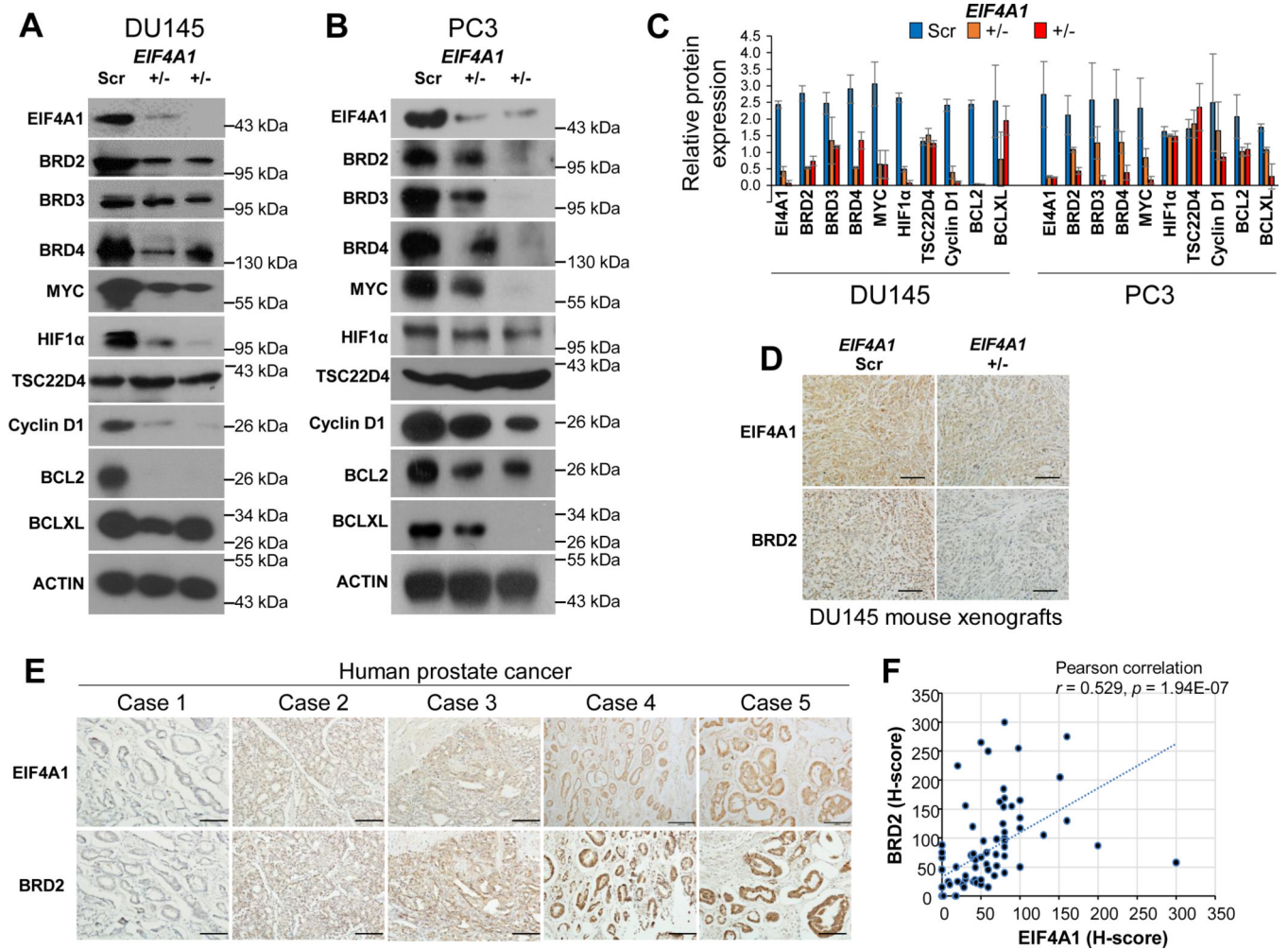
Figure 4. Relationship between expression levels of eIF4A1 protein and its potential target genes in human prostate cancer.

(**A-C**) Protein expression and quantitative analysis of eIF4A1 and its potential target genes in DU145 and PC3 cells, as determined by Western blots. Data are presented as the means and SD. * $p < 0.05$ by ANOVA followed by Tukey's *post hoc* test *vs.* the scramble control group. (**D**) Protein expression of eIF4A1 and DRD2 in DU145 xenograft tumors, as determined by IHC. (**E, F**) Protein expression and H-score analysis of eIF4A1 and BRD2 in primary prostate cancer tissues as determined by IHC. Scr, scramble. All experiments were repeated three times.